Rotary travelling wave oscillator with differential nonlinear transmission lines

Mabel Pontón, *Member IEEE*, Almudena Suárez, *Fellow IEEE*, J. Stevenson Kenney, *Fellow IEEE*

***Abstract*— A methodology for the harmonic-balance analysis and design of rotary-traveling wave oscillator (RTWO) is presented. Two different implementations are compared. The first one is the standard configuration based on a distributed transmission lines. The second one is a new configuration based on a differential nonlinear transmission line (NLTL), which enables the generation of square waveforms with reduced number of stages, while still maintaining the capability to produce multiphase signals. The possible coexistence of oscillation modes is investigated with a detailed bifurcation analysis versus practical parameters such as the device bias voltage. The phase-noise spectrum is predicted from the variance of the common phase deviation. The parameters that determine this variance are identified with the conversion-matrix approach. The two prototypes, based on a distributed transmission line and a differential NLTL, have been manufactured and characterized experimentally, obtaining very good agreement between simulations and measurements.**

Index Terms— Rotary traveling-wave oscillator (RTWO), harmonic balance (HB), differential nonlinear-transmission line (NLTL), stability, bifurcation, phase noise

I. INTRODUCTION

EMERGING communication standards demand signal sources with multiple phases. In a conventional approach the multiphase oscillation signals are generated through the coupling of LC-tank oscillators [1]-[8]. Recently the rotary-traveling wave oscillator (RTWO) has been proposed for high frequency clock generation [9]-[15], which is able to provide quasi-square signals with low phase noise. The basic RTWO architecture is a Möbius-ring-like differential transmission line with gain stages periodically distributed along the path. With a sufficient number of gain stages it is possible to obtain quasi-square waves, such that the rise and decay times decrease with the number of stages [15].

This work has been supported by the Spanish Ministry of Economy and Competitiveness through project TEC2011-29264-C03-01.

M. Pontón and A. Suárez are with the Dpto. de Ingeniería de Comunicaciones, Univ. de Cantabria, Santander, Spain (mabel.ponton@unican.es almudena.suarez@unican.es). J.S. Kenney is with the ECE at Georgia Institute of Technology in Atlanta, Georgia, USA. (jskenney@ece.gatech.edu).

The oscillation frequency ω_o is given by the travel time of the wave around the closed loop with the Möbius twist. In the desired oscillation mode, phase shift $2\pi/(2N)$, where N is the number of stages, is obtained between consecutive nodes, with 180º phase shift between equivalent nodes of the differential lines. In an RTWO, the wave propagates in one direction only and unlike LC-tank oscillators it is not susceptible to mismatching effects. In addition, the distributed nature of this oscillator alleviates the effects of the transistor parasitics [9] and therefore enables lower phase-noise spectral density. Another significant advantage is that accurate differential quadrature outputs needed for I/Q modulation and demodulation can be obtained at the fundamental oscillation frequency. With traditional oscillators, quadrature outputs are usually obtained by designing an oscillator circuit to produce twice the desired frequency, then using frequency dividers and other digital logic to obtain the quadrature outputs.

In most previous works [9]-[12] the design is based on either approximated expressions or time domain simulations of the multidevice architecture. However, the work [16] presents a harmonic-balance (HB) analysis of the RTWO, which enables an accurate modeling of the transmission lines and a numerically efficient determination of the steady-state regime. Here a methodology for the HB analysis and design of RTWOs is presented, which is combined with continuation techniques to analyze the evolution of the steady-state solution versus practical parameters such as the device bias voltages. The mechanisms for the possible generation of undesired oscillation modes are investigated and related to the symmetry properties of the oscillator configuration. Bifurcation relationships derived from the central-manifold theorem [17] and stability analysis based on pole-zero identification will be applied to the dc solution and to each of the possible periodic oscillation modes. In the case of periodic regimes, a small-signal current source at a frequency Ω incommensurable with the fundamental frequency ω_o of the periodic regime is introduced into the circuit, calculating the closed-loop transfer function $Z(\Omega) = V(\Omega)/I(\Omega)$ [18-19] with the conversion-matrix approach [20]. This involves replacing the nonlinear devices with their conversion matrixes and evaluating the linear network at the sideband frequencies $k\omega_o+\Omega$, where k is an integer going from –NH to NH. In [19] the poles obtained through the identification of $Z(\Omega)$ have been demonstrated to formally

agree with the Floquet exponents of the periodic solution for harmonic order |NH| tending to infinite.

With the aim to reduce the number of stages required to achieve a square waveform a new configuration based on the use of a differential nonlinear transmission line (NLTL) is proposed. The differential NLTL [18] is usually implemented with short transmission line sections and varactor diodes connected across the lines with a periodic distribution [19]-[24]. Due to the nonlinear characteristic of the diodes, propagation velocity increases with the signal amplitude. In a differential operation this enables a reduction of both rise and fall times, unlike the case of conventional single-ended NLTL, which only provides fall time reduction. As will be shown, this property will enable a useful reduction of gain stages and therefore a reduction of power consumption and phase noise.

The HB simulation of the RTWO enables the application of frequency-domain techniques for phase noise analysis. In the conversion-matrix approach [20],[25], the phase noise at a particular node and harmonic frequency k is obtained from the voltage phasors $V(k\omega_o+\Omega)$ and $V(-k\omega_o+\Omega)$. Thus, the analysis basically relies on the calculation of the linearized response of the node voltage to the noise sources. This analysis will implicitly account for any near-critical circuit pole, with impact on the noise-analysis bandwidth. However, this method, due to its inherent linearity, cannot predict the effect of the perturbed-oscillator nonlinearity in the common phase noise [26-32], associated to the carrier modulation, which affects the near-carrier phase noise. Here a calculation of the phase-noise spectrum from the variance of the common-phase deviation is applied to RTWOs for the first time to our knowledge. The analysis is based on the identification of the parameters that determine this variance [26] from simulations performed with the conversion-matrix approach [20], [25].

The paper is organized as follows. Section II presents the HB analysis of the RTWO. Section III shows the configuration of the RTWO with differential nonlinear transmission lines. Section IV is devoted to the stability and bifurcation analysis of this oscillator topology with emphasis on the detection of possible coexistent oscillation modes. Section V describes the phase-noise analysis based on the calculation of the variance of the common-phase deviation.

II. HB Analysis of the RTWO

The design based on a linear transmission line is sketched in Fig. 1(a). Two gain stages (N = 2) are initially considered, with phase shift between consecutive nodes $360^o/(2N) = 90^o$. For maximum flexibility, a hybrid demonstrator has been developed here, which uses an amplification stage based on the FET transistor NE3210S01. This particular choice is due to the availability of an accurate nonlinear model for this device. Fig. 1(b) shows the gain stage ($-G_m$), which must have identical effect for both propagation directions. To fulfill this requirement, a differential amplifier is used here. The balun imposes the 180º phase shift between the differential outputs (V_{o1} and V_{o2}). The selected bias point is V_{GS}= -0.5V and V_{DS} = 2.7 V. The inductance L_{gg} is optimized to obtain the negative resistance that should enable the self-sustained oscillation.

The desired oscillation frequency is f_o = 660 MHz. The total length of the transmission line must give rise to a total phase shift along the loop of 360º at this frequency. For an initial estimation of the total physical length, each line section is optimized separately from the circuit, in order to get a phase shift of 90º. The layout of the distributed-line prototype is shown in Fig. 2. Buffers have been used to extract the signals in the experimental characterization of the prototype. Each voltage buffer is designed using a single-stage NE3210S01 FET transistor in common-drain configuration. The initial RTWO design has been analyzed and corrected with harmonic balance. Due to the circuit symmetry, in the design with N = 2 gain stages, the multiphase mode coexists with an undesired in-phase mode, as will be demonstrated later.

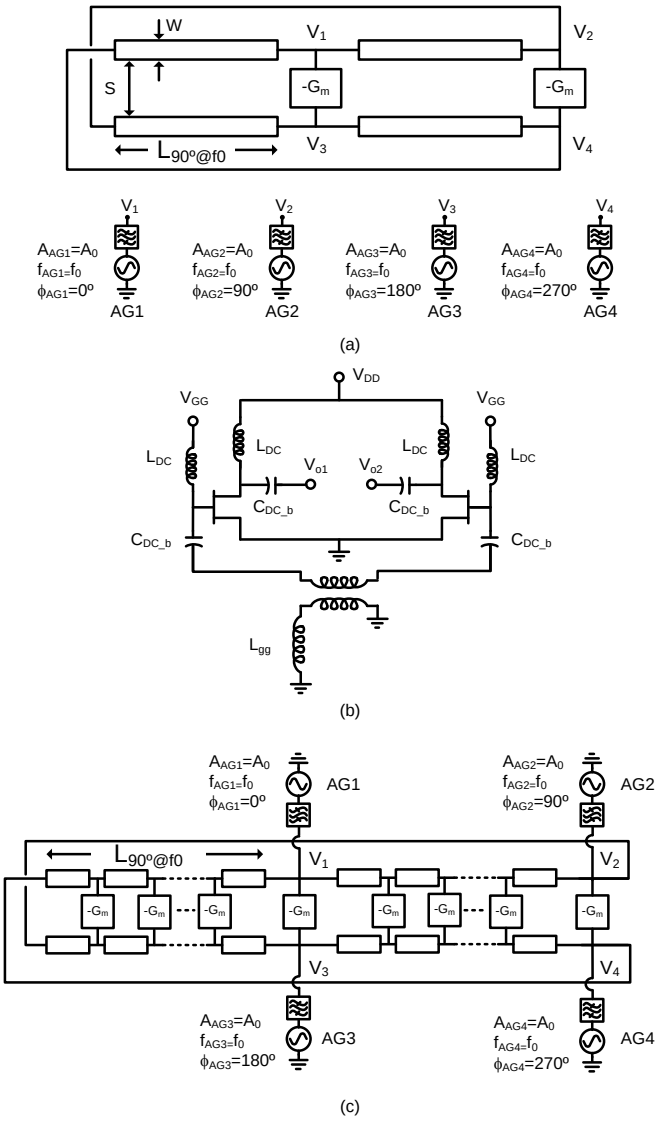

Figure 1 Distributed-line RTWO. (a) Schematic with N = 2 gain stages ($-G_m$) distributed-line RTWO showing the connection of the auxiliary generators. (b) Design of the gain stage ($-G_m$) using a differential amplifier based on FET NE3210S01 transistors. (c) Analysis procedure for any even number N>2 of gain stages, based on the use of four AGs only, with 90º phase shifts.

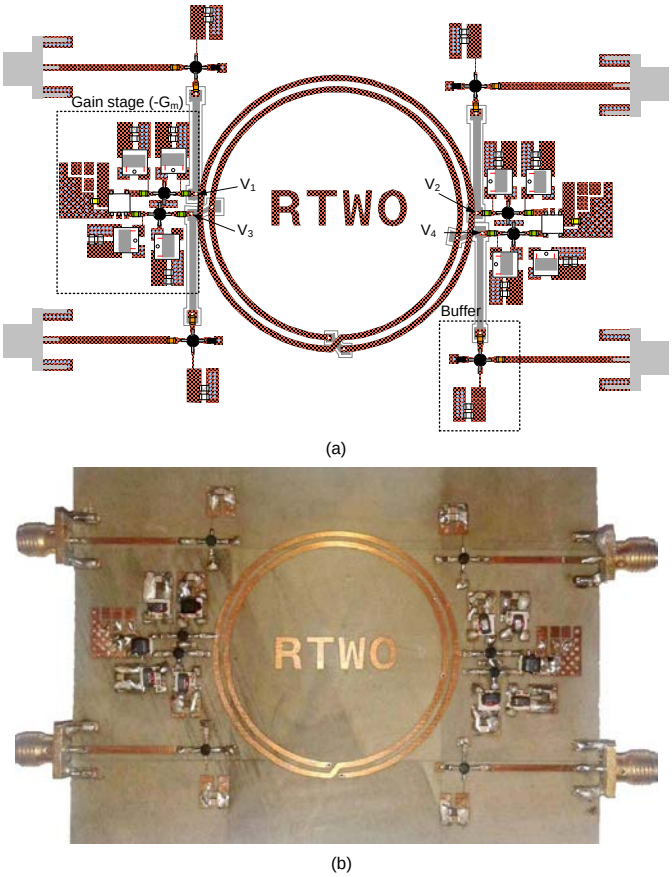

Figure 2 Distributed-line RTWO. (a) Layout. (b) Photograph of the double-sided prototype built in Rogers 4003C substrate. The FET transistor is NE3210S01.

The RTWO has been designed using the auxiliary-generator (AG) technique [33-36], adapted to the RTWO configuration. An AG is connected in parallel at each of the two nodes of the gain stages [see an example in Fig. 1(a)]. A set of n_{AG} non-perturbation conditions $Y_{AG,i}=0$, where i=1 to n_{AG}, are solved simultaneously in terms of the AG amplitudes and frequency or the AG amplitudes and some design parameters. This method has two advantages: (i) it avoids undesired HB solutions having any of the gain stages in a non oscillatory state and (ii) it allows presetting node-voltage phase shifts, consistent with each possible oscillation mode. Due to the RTWO symmetry, it is reasonably assumed that the oscillation modes have the same amplitude. Exceptions would come from the HB inability to excite the oscillatory solution at some of the gain stages, which would exhibit a positive real part of the current-to-voltage ratio at the oscillation frequency. Thus, the n_{AG} auxiliary generators will have the same amplitude $A_{AG} = A_o$ and the same frequency $\omega_{AG} = \omega_o$. The respective phase values $\phi_{AG,i}$, where i=1 to n_{AG}, are fixed and determined by the phase shifts of the particular mode (see Section IV). Note that due to the autonomy of the oscillatory solution the phase origin can be arbitrarily set to 0º.

The set of non-perturbation conditions $Y_{AG,i} = 0$, where i=1 to n_{AG}, constitutes an outer-tier equation system, with the pure HB system being the inner tier. This outer-tier system can be solved through error-minimization algorithms, such as Newton-Raphson, or using the commercial-HB software optimization tools. The initial RTWO design is carried out estimating the lengths of the transmission-line sections so as to have total 360º phase shift across the loop at the desired oscillation frequency ω_o. This frequency value can be imposed to the large-signal steady-state oscillation by setting $\omega_{AG} = \omega_o$ and optimizing the amplitude A_{AG} and one or more design parameters so as to fulfill the non-perturbation conditions $Y_{AG,i}=0$, where i=1 to n_{AG}, simultaneously. In the design of Fig. 1(a) the optimized parameter is the length of the transmission-line sections.

In the case of the multiphase solution, phase values at consecutive nodes (on the same side of the differential configuration) are given by $\phi_m = m2\pi/(2N)$, with m = 0 ... 2N-1. Therefore the phase shift between consecutive nodes decreases with N as $2\pi/(2N)$. For any even number of stages N>2, it has been possible to obtain the multiphase solution using only n_{AG}=4 AGs, in all the RTWO designs carried out here. With only four AGs at the critical phase values 0º, 90º, 180º and 270º, the configuration is divided into four equal sections [see Fig. 1(c)], with small phase-shift per gain stage. This critical choice of the AG locations, together with the small phase shift per stage, allows the multiphase solution to be maintained across the entire closed loop, avoiding any of the other possible modes. Tests have been carried out up to N = 64 gain stages always converging to the multiphase solution.

The situation is different for modes with larger phase-shift values, giving rise to a total phase shift $n360º$ across the loop, with n a positive integer. In general, for the analysis of those solutions, one AG should be connected between each node of the two nodes of each of the gain stages and ground. In the case of the multiphase solution, due to the symmetry properties of the RTWO configuration, the outer-tier system can be solved with a low computational cost. This is due to two facts. First, under symmetries, the phase shifts between the AGs remain identical, at the same values, during the whole convergence process. Second, the set of unknowns is quite limited, given by the AG amplitude, which is equal for all the AGs, and the oscillation frequency $\omega_{AG} = \omega_o$ or a suitable design parameter. Note that in the symmetrical case there are terms that are repeated in the matrixes modeling the passive and active components. Examples will be shown in Section IV, devoted to the stability analysis.

The method described has been applied for the design of a conventional RTWO based on the use of a distributed transmission line. The number of gain stages is N=2. As shown in Fig. 1, four AGs have been used, with phase values $\phi_{AG,m} = m2\pi/4$, with m = 0 ... 3. To ensure a steady-state oscillation of the RTWO at the desired frequency ω_o, the AG frequency is fixed $\omega_{AG} = 2\pi f_o$ (where f_o = 660 MHz) and the non-perturbation conditions are solved through optimization of the transmission-line length and the common amplitude $A_{AG} = A_o$.

Fig. 3(a) shows the voltage waveforms at the four nodes of the gain elements (see Fig. 2) when taking into account the influence of the non-ideal output buffers. As can be seen, they exhibit the desired 90º phase shift. Fig. 3(b) shows the

differential output voltages. The RTWO has been experimentally characterized using an Agilent 90804A Digital Storage Oscilloscope and an E4446A PSA Spectrum Analyzer. In Fig. 3(a) and Fig. 3(b), the measured waveforms can be compared with the simulated ones. For the same parameter values, the default HB solution (provided by the commercial software) exhibits very low amplitude at two of the output nodes, which is due to the inability of default HB analysis (which uses either only one oscport or probe or two oscillation-analysis nodes) to excite the oscillatory solution at all the gain stages (Fig. 4). Indeed, one of the gain stages exhibits a positive value of the real part of the current-to-voltage ratio at ω_o. In other cases, such as when varying a bias voltage or other parameters, default HB (applied to the design with N=2 gain stages) converges to an in-phase solution. This in-phase solution corresponds to zero phase values in all the $-G_m$ nodes connected by one of the two differential lines and 180° phase shift in all the $-G_m$ nodes connected by the other line [Fig. 5(a)]. In some preliminary designs (different from the one in Fig. 2), the undesired in-phase mode was stable and this is why it could be obtained with time-domain integration. In Fig. 5(b) the time-domain simulation of this stable solution is presented. Note that this preliminary design (in which the in-phase solution was stable) was discarded due to lack of interest. The stability of both the multiphase and the in-phase solution, which are the two fundamental modes of the RTWO with N = 2 gain stages, will be investigated in Section IV. It is possible to advance at this point that the multiphase solution is stable and the in-phase solution is unstable.

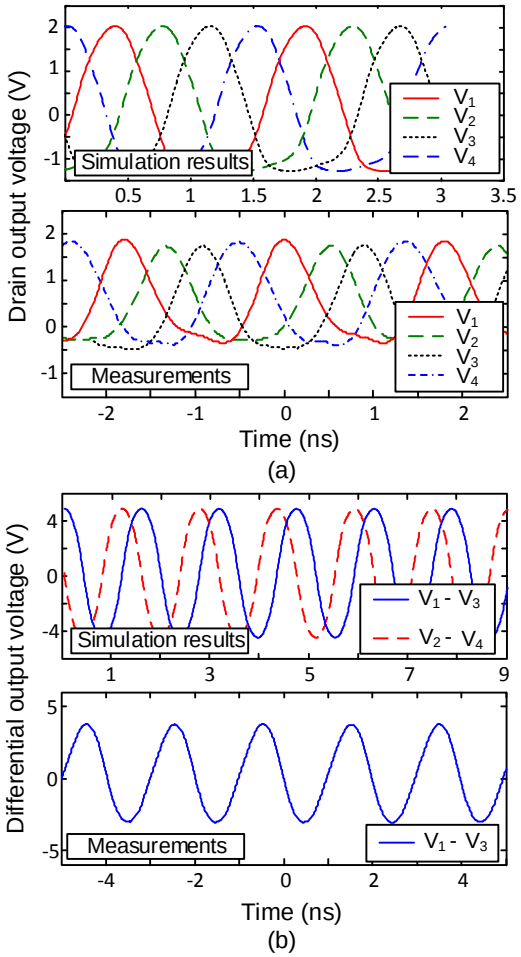

Figure 3 Distributed-line RTWO with N = 2. Comparison between measurement and simulated output waveforms when considering the output buffers. (a) Drain output voltages. (b) Differential output voltages.

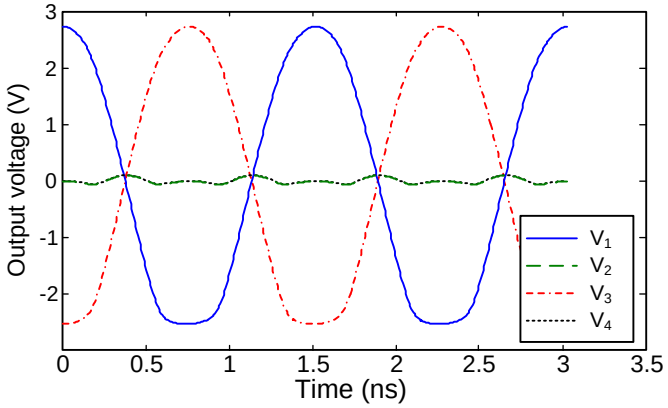

Figure 4 Distributed-line RTWO. Output voltages using default HB analysis. One of the waveforms has very low amplitude due to the inability of default HB to excite the oscillatory solution at all the gain stages.

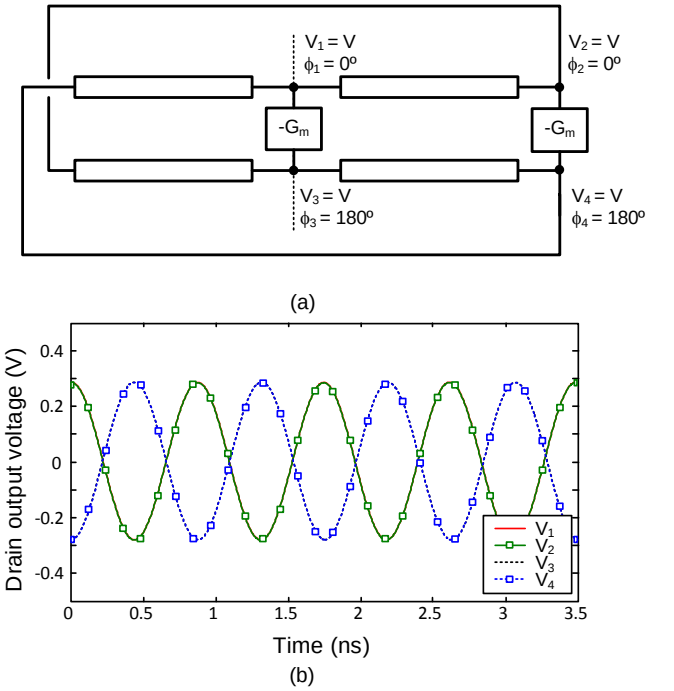

Figure 5 Undesired in-phase mode, obtained with two gain stages. (a) Phase values along the RTWO. (b) Waveforms obtained with a time-domain analysis in a preliminary design, different from the one in Fig. 2.

With the conventional RTWO based on a linear transmission line, the waveforms obtained for two gain stages (N=2) are quasi-sinusoidal (Fig. 3). In fact, to obtain quasi-square waveforms, the number of gain stages must be increased. Limitations in the harmonic-generation capability of the gain stage in Fig. 1(b) make the formation of the quasi-square waveform difficult. Therefore, this particular analysis has been carried out with the cross-coupled inverters proposed in [12]. In the case of N=2, the same line lengths of the RTWO design based on the gain stage in Fig. 1(b) are taken as an initial value for the AG optimization, with the oscillation frequency kept constant thanks to the use of the AGs. Indeed, the AG frequency is kept at the desired value $\omega_{AG} = \omega_o$, optimizing the AG amplitude A_{AG} and the line length so as to fulfill the non-perturbation conditions. Considering 20 harmonic components, only a small variation of the initial line length is observed after the convergence process. This is because the RTWO oscillation frequency is mostly determined by this transmission-line length. Fig. 6(a) shows the waveforms at the nodes with 90º phase shift, obtained when increasing the number of gain stages from N = 2 to N = 2^3 = 8. For each N>2, the initial length l(N) of the transmission-line sections is estimated by doing l(N-1)/2. This initial value is then corrected with the AG technique, suing only four AGs, with frequency set to the desired oscillation frequency $\omega_{AG} = \omega_o$.

III. Configuration of the RTWO with Differential Nonlinear Transmission Lines

As shown in Fig. 6(a), with the conventional RTWO implementation, based on a distributed transmission line, eight gain stages are necessary to obtain a quasi-square waveform. In order to reduce the number of required stages, the possible use of a differential nonlinear transmission line (NLTL) [18], instead of the distributed line, has been investigated here for the first time to our knowledge. The sections of differential NLTL will replace the distributed-line sections of the original topology. The differential NLTL is usually implemented with balanced short transmission line sections periodically loaded with reverse-biased varactor diodes [22-24]. This implementation, with one varactor diode per cell, is not possible in an RTWO topology due to the inversion of the varactor bias voltage at the Möbius twist, which breaks the symmetry of the configuration. To preserve the symmetry, anti-parallel varactor diodes [Fig. 7(a)] are used for the implementation of the differential NLTL. These diodes are dc-decoupled to ensure the reverse biasing. The chosen varactor diode is the hyper abrupt SMV1231 reverse biased at 4.8 V. Unlike the conventional single-ended NLTL, which sharpens either the front portion or the back portion of the pulse, a differential NLTL [21] can sharpen both portions with the resulting reduction of rise and fall times (see Fig. 6(b), using only N = 2 gain stages). This is a very convenient approach to obtain well-defined square signals with a relatively small number of gain stages. The NLTL-prototype layout and photograph are shown in Fig. 7(b) and Fig. 7(c), respectively. The gain stage is the same that the one used in the distributed-line RTWO design [Fig. 1(b)]. Each section of distributed transmission line has been replaced by three differential-NLTL cells, composed by a short inductive transmission line and a pair of anti-parallel varactor diodes. Eight buffers have been connected to extract the signals along the differential NLTL cells.

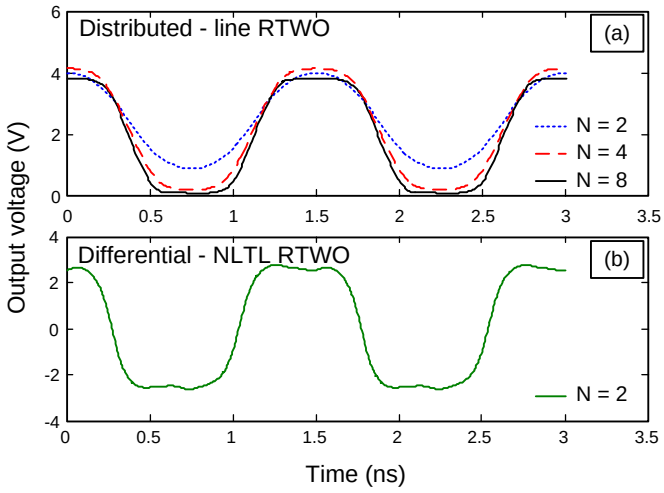

Figure 6 Comparison of output voltages. (a) Distributed-line RTWO with N = 2, 4 and 8 gain stages based on cross-coupled inverters. (b) Differential-NLTL RTWO with N = 2 using the gain stage in Fig. 1(b).

The varactor diodes are modelled with a Taylor series to facilitate the HB convergence. In fact, due to the complex topology of the RTWO, convergence was impossible with the standard junction-capacitance model of the hyper-abrupt diode. This is attributed to exponential functions in the diode model under forward operation, which are undesirably reached at some iterations of the convergence process, even though in the actual steady-state solution the forward excursion is negligible.

Instead, a sixth order Taylor series expansion is used, providing sufficient accuracy and facilitating the HB convergence. The coefficients are given by:

$$C_N = 2\left(-MC_{j0}\right)\left(-M-1\right)....\left(-M-N-1\right)\left(1-\frac{V_{varac}}{V_j}\right)^{(-M-N)}\left(\frac{-1}{V_j}\right)^N\frac{1}{N!} \quad (1)$$

where C_{j0} is the zero-bias junction capacitance, M is the grading coefficient, V_{varac} is the varactor bias voltage, V_j is the junction potential and N the order of Taylor-series coefficient.

Due to the anti-parallel connection of the diodes, odd harmonic components are null, which leads to the generation of a square-wave instead of a pulsed wave. For an estimation of the NLTL parameter values, the NLTL sections are optimized separately from the RTWO structure in order to obtain 90º phase shift. In this analysis, the differential NLTL is terminated in its approximate characteristic impedance: $Z_c = \sqrt{L/C_{av}}$, where C_{av} is the average varactor capacitance. Then, the excitation frequency is fixed at the desired oscillation frequency ω_o and the length and bias voltages of the varactor diodes are tuned in order to obtain 90º phase shift. Once introduced into the oscillator, the length of the transmission-line sections is reoptimized in order to fulfill the steady-state oscillation conditions (imposed with the AGs) at the desired oscillation frequency. The AG frequency is fixed at $\omega_{AG}=\omega_o$, optimizing the AG amplitude and NLTL inductance and varactor-bias voltage, in order to fulfill $Y_{AG,i}=0$, with i=1 to 4 [Fig. 7(a)]. Fig. 8(a) shows the voltage waveforms at the NLTL cells 1a, 4a, 1b and 4b obtained without the output buffers. Fig. 8(b) shows the corresponding measured waveforms. The amplitude discrepancies are due to the influence of the non-ideal output buffers. This is proved in Fig. 8(c), which compares the measured output waveform at one of the gain stages and the waveform simulated with the output buffers. Although necessary to extract the signals, the buffers are not constitutive of the RTWO, so they have not been used in the simulations of the intrinsic RTWO behavior. The differential NLTL enables the formation of the quasi-square waveform with only two gain stages. This should be compared (Fig. 6) with the case of the distributed-line RTWO based on inverter stages, which requires 8 gain stages to provide similar rise and decay times.

The RTWO design based on the differential NLTL offers the interesting capability of providing similar waveforms with phase shift about 45º between particular nodes [Fig. 8(d)]. This phase shift can be obtained in a distributed-line RTWO with N = 4 gain stages but not in a distributed-line RTWO with N = 2. For comparison, Fig. 9(a) and Fig. 9(b) show respectively the phase values for the case of a distributed-line RTWO with N = 4 gain stages and a differential-NLTL RTWO with N = 2.

As in the case of the distributed-line RTWO, for N = 2, the multiphase solution coexists with the in-phase solution (Fig. 10). This in-phase solution is non-symmetrical, that is, it has different rise and decay patterns. The stability of the multiphase and in-phase solutions in both the distributed-line and differential-NLTL RTWO are analysed in the next section.

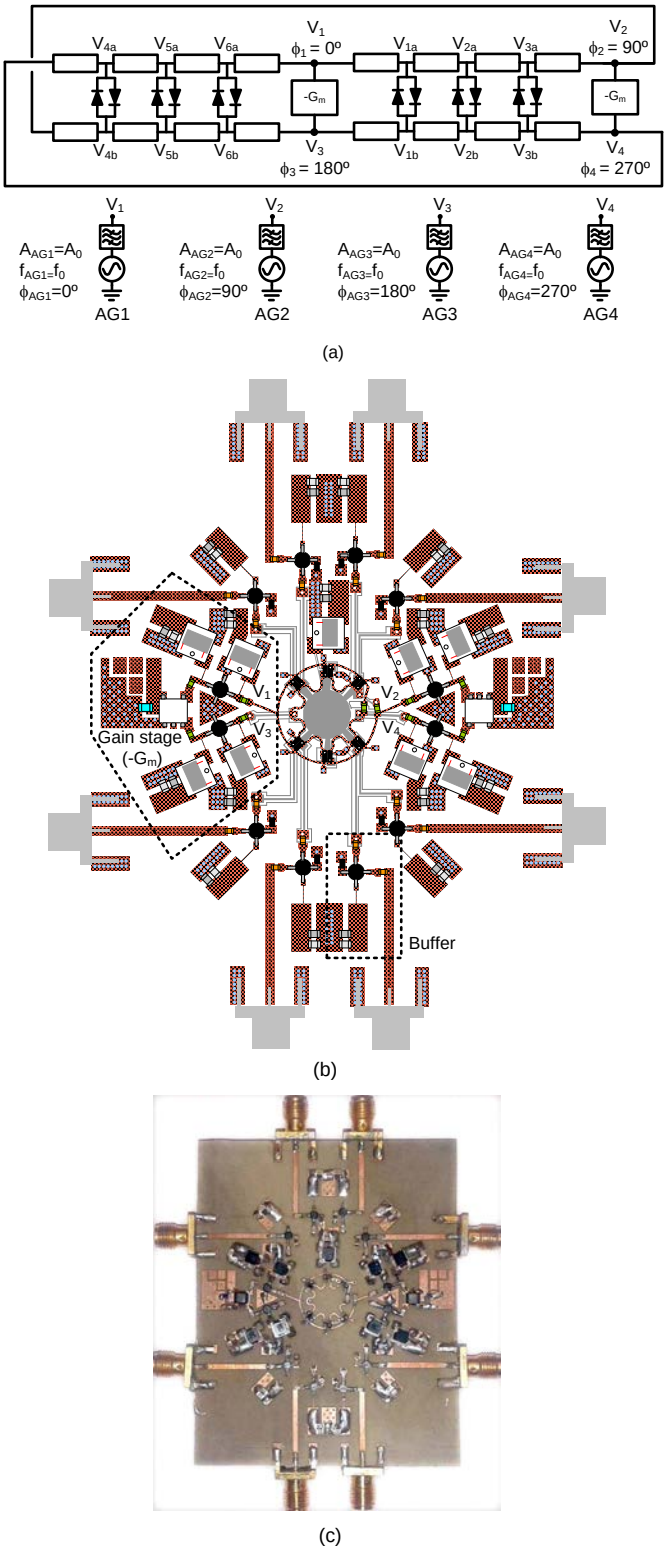

Figure 7 Differential-NLTL RTWO. (a) Schematic showing the anti-parallel connection of the varactor diodes, as well as the auxiliary generators used for the HB analysis and design. (b) Layout of the double-sided prototype based on a FET transistor NE3210S01. (c) Photograph of the prototype built in Rogers 4003C substrate

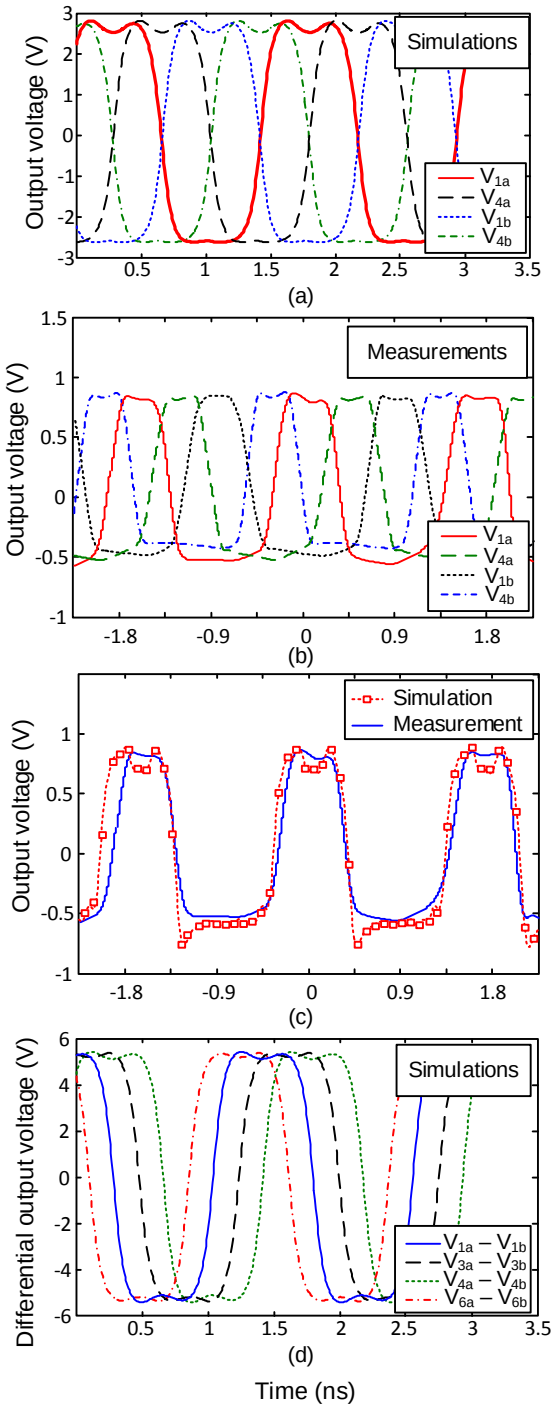

Figure 8 Differential-NLTL RTWO. (a) Simulated output voltages at the NLTL cells 1a, 4a, 1b and 4b. (b) Measured output voltages at the NLTL cells 1a, 4a, 1b and 4b. (c) Comparison between the measured output waveform at one of the gain stages and the waveform simulated with the output buffers. (d) Simulated differential output voltages at the NLTL at the nodes with phase shift 45º.

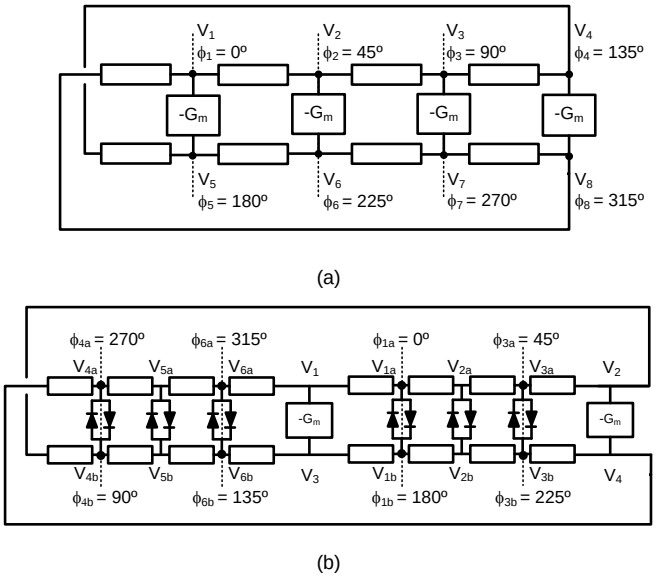

Figure 9 Phase values for: (a) Distributed-RTWO with N=4. (b) Differential-NLTL RTWO with N = 2.

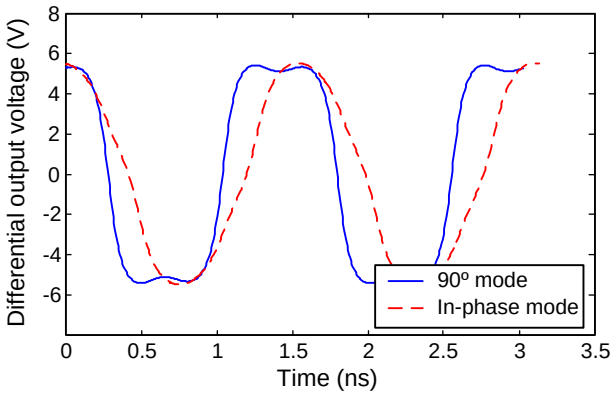

Figure 10 Differential-NLTL RTWO. Differential output voltage for the two different oscillation modes with N = 2 gain stages: 90º mode (solid line) and in-phase mode (dashed line).

IV. Stability Analysis

The generation of two or more modes (depending on the number of gain stages) can be explained from the symmetry properties of the circuit topology. Let reference planes be considered between the nodes of each gain stage, as shown in Fig. 1(a) (for the particular case of N=2). This allows modelling the oscillator circuit with two admittance matrixes, corresponding to the passive and active subnetworks respectively. In the general case of N gain stages, it is easily derived that the passive subnetwork admittance matrix is circular with 2N-3 zero values per row, whereas the active subnetwork admittance matrix is block-diagonal, with reciprocal submatrixes, due to the symmetric topology of the gain stages.

In the following, the case of N = 2 will be analyzed in detail, as both the distributed-line RTWO and the differential-NLTL RTWO designed here are based on N = 2 gain stages. Considering small-signal voltage excitations, the circuit equations are the following:

$$\left\{\begin{bmatrix} y_{11} & y_{12} & 0 & y_{12} \\ y_{12} & y_{11} & y_{12} & 0 \\ 0 & y_{12} & y_{11} & y_{12} \\ y_{12} & 0 & y_{12} & y_{11} \end{bmatrix} + \begin{bmatrix} Y^a_{11} & 0 & Y^a_{13} & 0 \\ 0 & Y^a_{11} & 0 & Y^a_{13} \\ Y^a_{13} & 0 & Y^a_{11} & 0 \\ 0 & Y^a_{13} & 0 & Y^a_{11} \end{bmatrix}\right\} \begin{bmatrix} V_1 \\ V_2 \\ V_3 \\ V_4 \end{bmatrix} = \begin{bmatrix} I_1 \\ I_2 \\ I_3 \\ I_4 \end{bmatrix} \quad (2)$$

Adding the two admittance matrixes one has a Topelitz matrix and a system of the form:

$$\begin{bmatrix} Y^a_{T,11} & y_{12} & Y^a_{13} & y_{12} \\ y_{12} & Y^a_{T,11} & y_{12} & Y^a_{13} \\ Y^a_{13} & y_{12} & Y^a_{T,11} & y_{12} \\ y_{12} & Y^a_{13} & y_{12} & Y^a_{T,11} \end{bmatrix} \begin{bmatrix} V_1 \\ V_2 \\ V_3 \\ V_4 \end{bmatrix} = \begin{bmatrix} I_1 \\ I_2 \\ I_3 \\ I_4 \end{bmatrix} \quad (3)$$

where $Y^a_{T,11} = y_{11} + Y^a_{11}$. Due to the circuit symmetry, equal amplitudes at the four observation nodes will be assumed. With both the multiphase excitation $[V\ Ve^{j\pi/2}\ Ve^{j\pi}\ Ve^{j3\pi/2}]^t$ and the in-phase excitation $[V\ V\ Ve^{j\pi}\ Ve^{j\pi}]^t$, the small-signal admittance observed from any of the four analysis nodes (n=1 to 4), when looking into the circuit, is the same and is given by:

$$Y_{Tn}(V=0,\omega) = Y^a_{T,11} - Y^a_{13} = y_{11} + Y^a_{11} - Y^a_{13} \quad (4)$$

which agrees with one of the eigenvalues of the total-admittance matrix in (3). This eigenvalue, with multiplicity two, is associated to two eigenvectors with equal-amplitude components and phase values corresponding to those of the multiphase and in-phase modes. Therefore, if the oscillation start-up conditions are fulfilled by the multiphase mode, they will equally be fulfilled by the in-phase mode. In this degenerate situation, the linear analysis of the dc bifurcation point cannot predict which of the two periodic modes generated is the stable one.

To check for the possible existence of other modes, a stability analysis of the dc solution of the distributed-line RTWO has been carried out using pole-zero identification [18-19]. This analysis is performed versus variation of the drain bias voltage V_{DD} of the devices used in each gain stage [Fig. 11(a)]. For small drain bias voltage, the dc solution is stable. At the bias voltage V_{DD}=0.224 V, this dc solution undergoes a double Hopf bifurcation (H). Two overlapped pairs of complex conjugate poles cross the imaginary axis to the right-hand side of the complex plane (RHP), associated to the eigenvalue with multiplicity 2, detected in (3)-(4). When further increasing the drain bias voltage no other poles cross the axis. The two pairs of poles should correspond to the multiphase and in-phase modes, generated at the same bifurcation point. For small discrepancies in the line lengths or any other elements, two ordinary Hopf bifurcations should occur at slightly different parameter values. This has been verified with the analysis in Fig. 11(b), performed for the case of a small discrepancy in the length of the transmission lines between the gain-stage sections. In this case, the dc solution undergoes two consecutive Hopf bifurcations (H_1 and H_2). The bifurcations in Fig. 11(a) and Fig. 11(b) will be studied in detail later in this section.

With a higher number N of gain stages, other modes with equal amplitudes and different phase distributions may exist. For instance, with N=4, modes with phase shifts $(2n+1)2\pi/8$, where n = 0 to 2 have been detected here. Unlike the case of N = 2 gain stages, the modes are generated at different parameter values, since they correspond to different eigenvalues of the total-admittance matrix of dimension 8 x 8, calculated in a manner similar to the 4 x 4 case considered in (3).

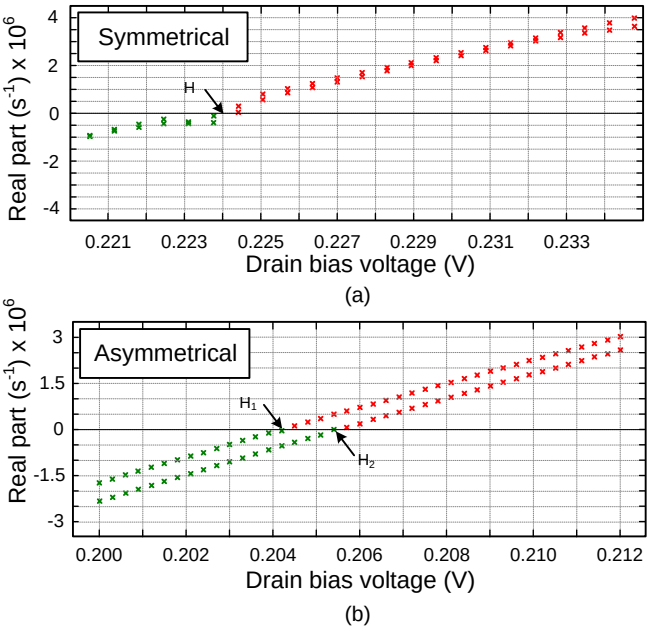

Figure 11 Distributed-line RTWO. Variation of the real part of the two pairs of dominant complex-conjugate poles versus the drain-bias voltage V_{DD}. (a) Totally symmetrical RTWO. (b) Slightly asymmetrical RTWO, with small discrepancies between the line lengths.

The following analysis focuses on the two modes detected in the RTWO with N=2 stages that has been designed and manufactured here. The steady-state oscillation curves corresponding to the multiphase and in-phase modes of the perfectly-symmetric distributed-line RTWO have been analyzed versus the drain bias voltage (V_{DD}). The in-phase solution is obtained using four AGs. These AGs will have zero phase value ϕ_{AG}=0º in one of the lines of the differential pair ($A_{AG}e^{j0}$) and ϕ_{AG}=180º in the other line ($A_{AG}e^{j180^\circ}$) [see Fig. 5(a)]. The results for the distributed-line RTWO are presented in Fig. 12. The bifurcation diagrams show the variation of the oscillation frequency [Fig. 12(a)] and the oscillation amplitude [Fig. 12(b)] versus V_{DD}. The in-phase and multiphase solutions are generated from zero oscillation amplitude at the same V_{DD} value [Fig. 12(b)], in agreement with Fig. 11(a) and with the analysis in (2) and (3). Then, the two solutions evolve in a different manner, resulting in different frequency and amplitude curves versus V_{DD}. This is because, as expected, when increasing the excitation amplitude, the response of the active subnetwork does depend on the phase shift between the node voltages. The cases of strong and weak coupling of the differential transmission line have been considered. In the case of strong coupling, as the parameter V_{DD} shifts from the bifurcation point, there are bigger differences between the oscillation frequencies of the multiphase and in-phase modes. As will be shown, only the multiphase solution is stable. Measurements corresponding to this solution are superimposed with good agreement.

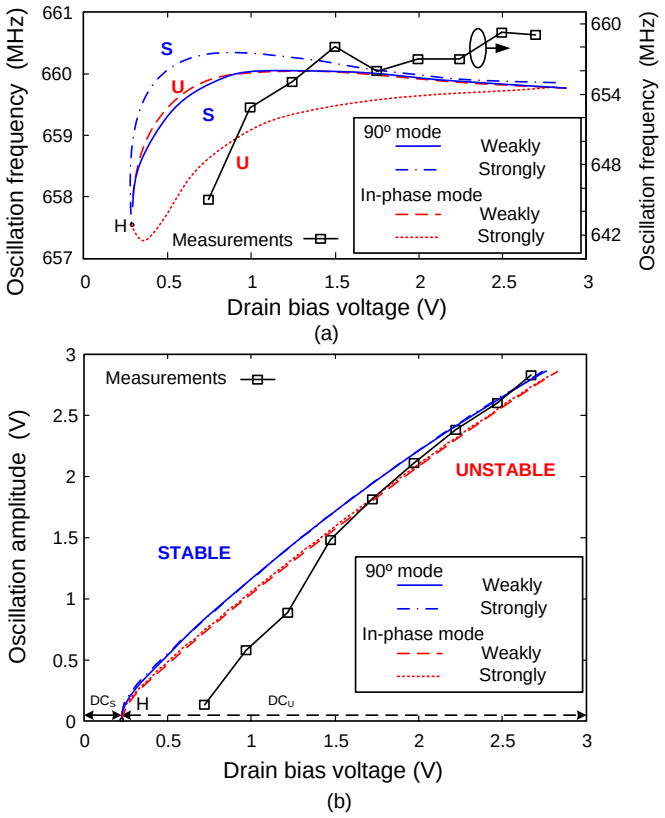

Figure 12 Distributed-line RTWO. Bifurcation diagram of the RTWO versus drain-bias voltage for weakly-coupled lines and strongly-coupled lines. (a) Variation of the oscillation frequency. (b) Variation of the oscillation amplitude at the drain nodes. Measurements are superimposed in the case of the stable multiphase solution.

For the bifurcation analysis, the simpler case of the slightly asymmetric 2 gain stages RTWO [Fig. 11(b)], undergoing two consecutive Hopf bifurcations (H_1, H_2), will be initially considered. The analysis will be based on bifurcation relationships, derived from the central manifold theorem [17]. At each Hopf bifurcation, a periodic solution is generated. The stability of periodic solutions is determined by a set of L Floquet multipliers m_1, m_2 to m_L, where L is the system dimension [37-38]. A stable periodic oscillation must have a real multiplier with value 1 (m_1=1), associated with the system autonomy, and the rest of its real and complex-conjugate multipliers must have magnitude smaller than one, that is, $|m_i|<1$, where i=2 … L-1.

The double Hopf bifurcation in the symmetric case (Fig. 12) is superciritcal [34] (the oscillatory solutions do not coexist with the dc regime prior to the bifurcation). Assuming that the small asymmetry does not change the nature (supercritical or subcritical) of the bifurcation, only this supercritical case will be considered. The first Hopf bifurcation H_1 in Fig. 11(b) occurs from a stable dc regime and taking into account the central manifold theorem the transformation must be the following [39]:

$$dc_0 \rightarrow dc_2 + P^{0,1} \qquad (5)$$

where dc means dc solution and the subindex indicates the number of poles of the dc solution on the RHP. In the same expression, P indicates periodic solution and the superindexes indicate the number of multipliers with magnitude larger than one and the number of multipliers with value one, in this order. Therefore, the periodic solution generated from a stable dc solution will be stable too (at least in the neighbourhood of the bifurcation). The second Hopf bifurcation H_2 in Fig. 11(b) takes place from an unstable dc regime dc_2, and the bifurcation relationship is the following [39]:

$$dc_2 \rightarrow dc_4 + P^{1,2} \qquad (6)$$

which corresponds also to a supercritical bifurcation [34]. The periodic solution generated from an unstable dc regime will be unstable in the neighborhood of the bifurcation. Indeed, the unstable pair of complex-conjugate poles existing in the dc solution (different from the one that gives rise to the oscillation) equally affects the stability properties of the periodic solution, which has small amplitude in the near the bifurcation point. Because the circuit is not perfectly symmetric in the case of Fig. 11(b), the two pairs of complex conjugate poles have a different frequency, and the unstable pair of complex-conjugate eigenvalues of the dc solution will give rise to a pair of complex-conjugate multipliers in the periodic oscillation.

In the degenerate case [Fig. 11(a)], two pairs of poles of the dc solution will cross the imaginary axis at the same parameter value. This non-structural bifurcation is obtained with perfect symmetry properties in the RTWO topology. The bifurcation relationship is the following:

$$dc_0 \rightarrow dc_4 + P^{1,1} + P^{0,1} \qquad (7)$$

Because the frequency of the two pairs of crossing poles is the same (ω_o) at the degenerate Hopf bifurcation, at this point there will be two coincident periodic solutions with oscillation amplitude tending to zero. Immediately after the bifurcation [relationship (7)], the two solutions split, both having one multiplier $m_1 = 1$, associated to the oscillation autonomy. In one of the periodic solutions ($P^{0,1}$), all of the other multipliers have magnitude smaller than one. In the other solution ($P^{1,1}$), one of the real multipliers is larger than one. In the case analyzed, pole-zero identification [18-19] shows that the stable solution of type $P^{0,1}$ is the multiphase solution and the unstable solution of type $P^{1,1}$ is the in-phase solution. In both solutions, three pairs of complex-conjugate poles at the oscillation frequency ω_o have been detected (Fig. 13). Associated to each Floquet multiplier m_i, there is an infinity of poles, satisfying the relationship $m_i = e^{p_{i,k}T}$, where T is the solution period, $p_{i,k}=p_i+k\omega_o$ and k is an integer. Therefore, a number of pairs of complex-conjugate poles at the oscillation frequency ω_o corresponds to the same number of real Floquet multipliers. Therefore, three dominant real multipliers m_1, m_2, m_3 have been detected with pole-zero identification in the two solutions [Fig. 13(a) and Fig. 13(b)]. The existence of more than one dominant real multiplier (in addition to the one associated with the solution autonomy $m_1 = 1$) is a consequence of the double Hopf bifurcation and the preservation of the dimension of the critical subspace. In both the multiphase and the in-phase solution, one of the two pairs of complex-conjugate poles corresponds to the solution autonomy. It should be exactly on the axis but unavoidable identification errors give rise to a small shift to the left-hand side.

As gathered from Fig. 13(a), the dominant real multipliers of the multiphase solution satisfy m_1=1, m_2<1 and m_3<1, with m_2>m_3, whereas those of the in-phase solution satisfy m_1=1, m_2>1 and m_3<1. At the degenerate Hopf bifurcation, the two solution paths merge (Fig. 12) and an infinite-slope point is clearly observed in the frequency curve [Fig. 12(a)], where the multiplier m_2 passes through 1, giving rise to a singularity.

Fig. 14 presents the same bifurcation analysis carried out for the differential NLTL RTWO, which also fulfils the small-signal relationships in (3) and (4). In a manner similar to the distributed-line RTWO, the two solutions of the NLTL RTWO are generated at the same V_{DD} value. The multiphase solution is stable whereas the in-phase solution is unstable. Measurements corresponding to the multiphase mode are superimposed.

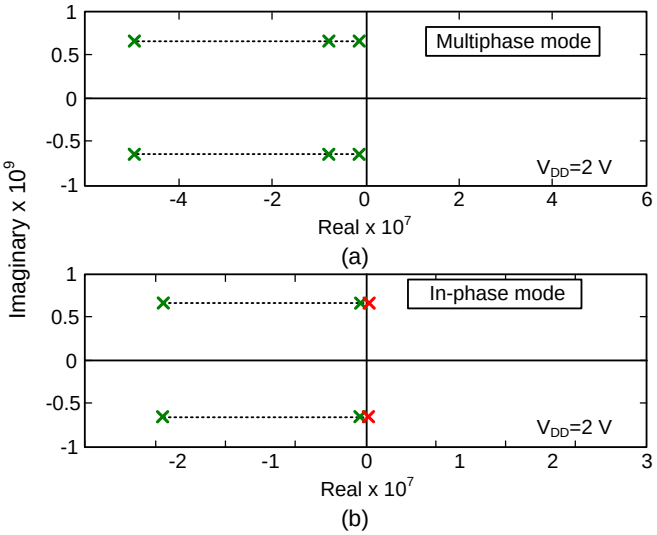

Figure. 13 Distributed-line RTWO. Stability analysis with pole-zero identification of the two coexistent oscillation modes. (a) Multiphase mode. (b) In-phase mode. In the two cases, the three pairs of dominant poles have the same frequency and this frequency is equal to the oscillation frequency.

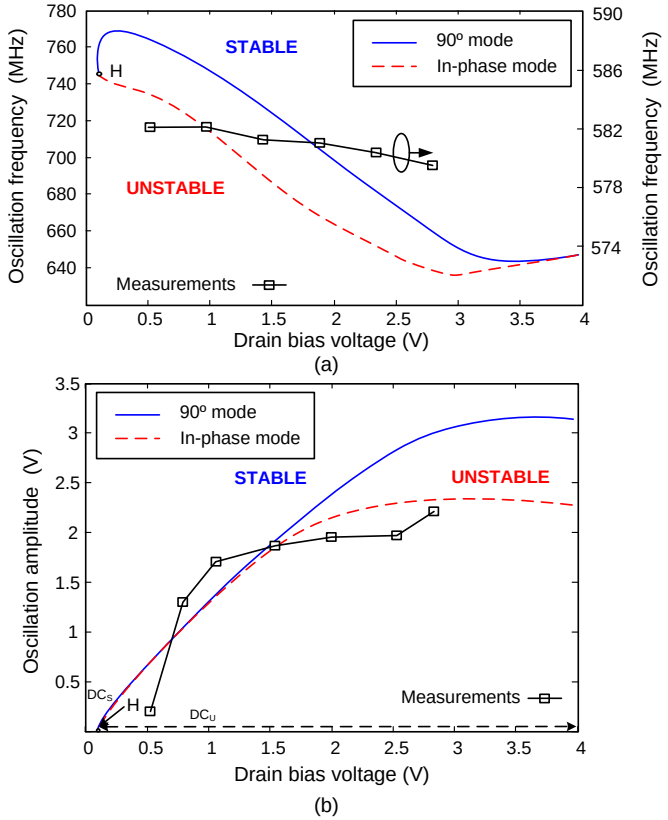

Figure 14 Differential-NLTL RTWO. Bifurcation diagram with N = 2 gain stages versus the drain-bias voltage for a varactor reverse bias voltage of 4.8 V. (a) Variation of the oscillation frequency. (b) Variation of the oscillation amplitude at the drain nodes. Measurements are superimposed in the case of the stable multiphase solution.

V. Phase-Noise Analysis

The HB simulation of the RTWO enables a phase-noise analysis with the conversion-matrix approach [20], [25]. All the modeled noise sources are considered and the possible impact of near critical poles on the noise spectrum is predicted, which enables a realistic simulation. However, accuracy degrades at low frequency offset due to ill-conditioning of the conversion matrix as the zero offset frequency is approached. This may be circumvented with the carrier-modulation approach [20], which removes the systems singularity replacing the imaginary part of one of the harmonics with the oscillation frequency. As shown in [20], in the intermediate range of offset frequencies, the results of the two methods are nearly equal, with differences being observed at low and high offset frequencies. However, due to their inherent linearity, none of these two methods take into account the nonlinearity of the perturbed oscillator with respect to the common phase deviation [23-32], associated to the timing noise [40] (or carrier modulation [20]). This nonlinearity mainly affects the phase-noise spectrum at low frequency offset from the carrier and gives rise to a flattening of the phase-noise spectral density.

In the following, a full analysis of the phase-noise spectrum of the RTWO based on the variance of the common phase deviation [26-28] will be presented. Unlike the works [26-28], the analysis is performed in the frequency domain, from a linearization of the HB system in the presence of noise

perturbations, performed with the conversion-matrix approach. The analysis is based on two facts. From certain offset frequency from the carrier, the method in [26]-[28] has been analytically demonstrated in [30] to be equivalent to the carrier-modulation approach [20]. Unless there are near-critical poles affecting the phase noise spectrum, results from the conversion-matrix approach and the carrier modulation approach will agree from sufficiently large offset frequency from the carrier [20].

Here the phase-noise spectrum will be calculated numerically from the variance $\sigma^2(t)$ of the timing noise $\theta(t)$ (associated to the common phase deviation), after identification of the parameters that determine this variance. Flicker noise sources in parallel between the intrinsic drain and source terminals and white noise sources are considered. The modulated flicker-noise source associated to each drain current $i_d(t)$ can be modeled [41] as $i_{d\_cyc}(t) = \beta \left(i_d(t)\right)^{\alpha} \varepsilon^F(t)$, with α, β constant coefficients and $\varepsilon^F(t)$, the elementary flicker process. The coefficients α and β are fitted through comparison with measurements in large-signal oscillating regime, as described in [41]. With a total of M flicker noise sources, the variance can be written [23]:

$$\sigma^2(t) = c_w t + \sum_{m=1}^{M} \left|V_{om}\right|^2 \int_{-\infty}^{\infty} S_F(f) \frac{1 - \exp(j2\pi f t)}{4\pi^2 f^2} df \qquad (8)$$

where $f = \Omega / 2\pi$ is the offset frequency from the carrier and $S_F(f)$ is the flicker noise characteristic 1/f. The constant value c_w depends on the sensitivity function with respect to the white-noise sources and the correlation matrix of these noise sources. Finally, V_{om} with m=1 to M is the dc value of the effective phase-sensitivity functions with respect to each flicker noise source. This effective function is obtained from the product of the "intrinsic" sensitivity function (relating the phase deviation to the small-amplitude current source) and the deterministic periodic term $\beta \left(i_d(t)\right)^{\alpha}$, as shown in [42-43]. In the numerical calculation of (8), a small corner frequency, in the order of 1 Hz, is introduced to avoid singularity in the integral [44]. Then, the phase-noise spectrum is obtained calculating numerically the following Fourier transform [26-28,44-45]:

$$S(f) = F\left\{\exp\left(-\frac{1}{2}\omega_o^2 \sigma^2(|\tau|)\right)\right\} \qquad (9)$$

The variance in (8) depends on c_w and $\gamma = \sum_{m=1}^{M} \left|V_{om}\right|^2 \alpha_m$. If there are no near-critical poles affecting the phase-noise spectrum, there can be identified from the phase-noise spectrum obtained with the conversion-matrix approach. Indeed, the work [26] analytically demonstrates that the two parameters c_w and γ, which determine the variance of the common phase deviation in (8), determine also the far from carrier phase noise. In the case considered here of white and flicker noise sources, this spectrum (at sufficiently large offset from the carrier) is given by:

$$S(f) = c_w \frac{f_0^2}{f^2} + \sum_{m=1}^{M} \left|V_{om}\right|^2 \alpha_m \frac{f_0^2}{f^3} = \frac{c_w f_0^2}{f^2} + \frac{\gamma f_0^2}{f^3} \qquad (10)$$

Unless there are system poles with small distance to the imaginary axis, the spectrum obtained with the conversion-matrix approach will exhibit the characteristic $S(f) = b/f^2 + a/f^3$, where "a" and "b" are constants. Then the values of γ and c_w can be identified from this spectrum. The two coefficients "a" and "b" are obtained from the spectral density at two different offset frequencies f_1 and f_2, solving the following linear system:

$$\begin{aligned} \frac{b}{f_1^2} + \frac{a}{f_1^3} &= S_1(f_1) \\ \frac{b}{f_2^2} + \frac{a}{f_2^3} &= S_2(f_2) \end{aligned} \qquad (11)$$

Then, γ and c_w are given by: $c_w = b / f_0^2$ and $\gamma = a / f_0^2$. It must be emphasized that for this method to be applicable the phase noise characteristic must correspond indeed to the one assumed $S(f) = b/f^2 + a/f^3$ and must be independent of the analysis node, so that it can be reasonably attributed to the common phase-noise deviation.

a) *Distributed-line RTWO*

The phase noise of the distributed-line RTWO (biased at V_{GS} = -0.5 V), is initially analyzed with the conversion matrix approach. The spectrum exhibits the usual characteristic $S(f) = b/f^2 + a/f^3$ and is independent of the observation node. The described analysis based on the calculation of the variance in (8) from parameters identified with the conversion-matrix approach is applicable and provides the spectrum represented with dashed line in Fig. 15 and Fig. 16, where it can be compared with the measured spectrum. The flattening of the near carrier phase noise is due to the nonlinearity with respect to the common phase-noise deviation and the preservation of the non-perturbed oscillator power under phase modulation only [26-28].

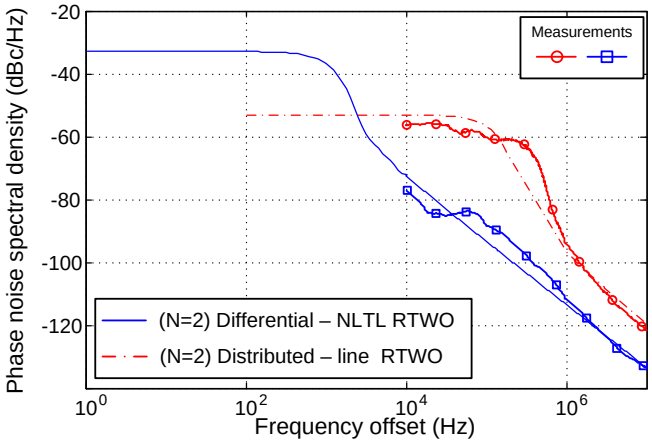

Figure 15 Comparison between the phase-noise spectra obtained from the variance of the phase deviation (10) with the distributed-line RTWO and with the RTWO designed using a differential NLTL. Modulated flicker-noise current sources have been considered in the two cases.

b) *NLTL RTWO*

The original NLTL RTWO design, with the transistor biased for some V_{GS} values, exhibited much higher phase noise values than the distributed-line RTWO. The spectrum corresponding

to V_{GS} = -0.8 V is shown in Fig. 16, with measurements superimposed. A slope of near -40 dB per decade can be noticed at relatively high offset frequency from the carrier, which is maintained for a long frequency interval. As shown in a recent work [32], this slope can be attributed to the presence of a negative real pole λ_2 of the steady-state oscillatory solution close to the imaginary axis. The effect of this pole on the phase-noise spectrum cannot be predicted with the Floquet decomposition used in [26-28]. In those works, a nonlinear scalar equation in the common phase deviation (or, equivalently, timing noise $\theta(t)$ due to the system autonomy) is decoupled from the perturbed-oscillator system. This is done by multiplying this system by the vector $\bar{v}_1^T(t)$ associated to the multiplier m_1=1 in the adjoint linearized system. With the resulting scalar equation it is not possible to predict the effect of possible near critical multipliers on the phase-noise spectrum. These near critical Floquet multipliers would, instead, affect the so-called amplitude perturbation, as shown in [28].

The existence of the near-critical pole λ_2 is explained as follows. At the Hopf bifurcation from dc regime [34] (obtained when varying a circuit parameter), the two complex conjugate poles that cross the imaginary axis transform into two real Floquet multipliers of unit value, or equivalently *two* set of poles of the form $0+k\omega_{in}$ where k is an integer. Then the periodic solution generated will have two 'canonical' poles at zero ($\lambda_1 = 0$ and $\lambda_2 = 0$) at the bifurcation point, where the oscillation amplitude tends to zero. One of them stays at zero ($\lambda_1 = 0$) for all the parameter values, since it is associated to the solution autonomy. When varying the parameter away from the Hopf bifurcation, the real pole λ_2 will generally grow quickly in magnitude. In other cases, like the one analyzed here, it remains at small value and gives rise to a slope of -40 dB per decade.

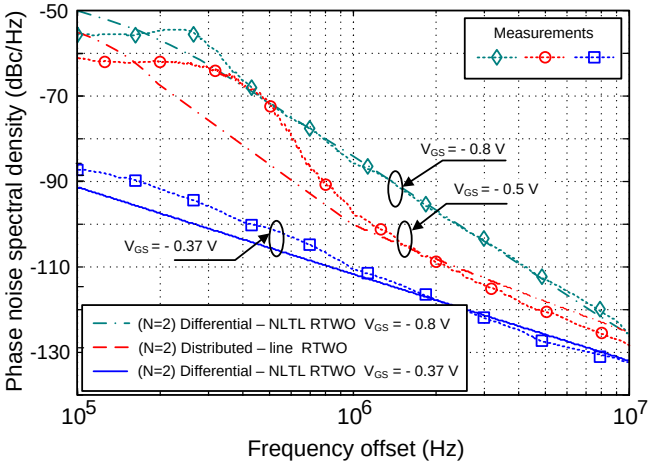

Figure 16. Phase-noise spectra measured with the N =2 gain-stage distributed-line RTWO and the N = 2 gain-stage NLTL RTWO proposed in this work for two different values of gate-bias voltage. For V_{GS}=-0.8 V the differential-NLTL RTWO exhibits an anomalous -40 dB/dec decay.

The high slope -40 dB/dec is obtained at relatively high offset frequency from the carrier. Therefore, for an analytical study of this behavior, it will be possible to carry out a simplified derivation, considering the influence of white-noise only. Note that the goal is not to perform an accurate phase-noise analysis (which is done here calculating the variance of the phase deviation) but to understand and correct the anomalous characteristic of the phase-noise spectrum. The solution, obtained with four AGs is given as initial value to a HB analysis with only one AG. This will provide a single outer-tier admittance function Y_{AG}, (equal to zero in the unperturbed free-running regime). This outer-tier admittance function is linearized about the free-running solutions calculating its derivatives with respect to the amplitude and frequency through finite differences [46]. Following the derivation in [32], relatively far from the carrier, the phase-noise spectrum is given by:

$$\left|\phi(\Omega)\right|^2 = \frac{\left[\left|Y_{TV}\right|^2 + \Omega^2 \frac{\left|Y_{T\omega}\right|^2}{V_s^2}\right]}{\Omega^2\left[\left|Y_{TV}\times Y_{T\omega}\right|^2 + \frac{\left|Y_{T\omega}\right|^4}{V_s^2}\Omega^2\right]} 2\left|I^w\right|^2 \quad (12)$$

where Ω is the offset frequency, Y_V and Y_ω are the admittance derivatives with respect to amplitude and frequency, calculated as described, and V_s is the amplitude of the steady state oscillatory solution. The cross product corresponds to $a\times b = \mathrm{Re}(a)\,\mathrm{Im}(b) - \mathrm{Re}(b)\,\mathrm{Im}(a)$. On the other hand, $\left|I^w\right|^2$ is the noise spectral density of an equivalent white-noise current source, connected at the AG location. From inspection of (12), the transfer function relating the phase-noise deviation to the current perturbation must have one pole λ_2 and one zero z. Their expressions, immediately derived from (12), are the following:

$$\lambda_2 = \frac{-\left|Y_{TV}\times Y_{T\omega}\right|}{\left|Y_{T\omega}\right|^2}V_s, \qquad z = \frac{-\left|Y_{TV}\right|}{\left|Y_{T\omega}\right|}V_s \quad (13)$$

From inspection of (13), the relationship $|\lambda_2| \le |z|$ is fulfilled, so for small $|\lambda_2|$, the spectrum will show a slope of -40 dB/dec. Low $|\lambda_2|$ will be obtained for small values of $|Y_{TV}\times Y_{T\omega}|$, which require non-negligible imaginary part of Y_{TV}. Because the pole λ_2 is associated to the imaginary part of Y_{TV}, the transistor bias point should be relevant. Taking this into account, the variation of the real pole with the gate bias voltage has been analyzed with both (13) and the conversion-matrix approach (Fig. 17). For V_{GS}=-0.37 V, the pole λ_2 is quite far from the axis. The change in the bias condition does not alter the quasi-square waveform, which is due to the action of the NLTL.

As verified with the conversion-matrix approach, for V_{GS} = -0.37 V, the spectrum exhibits the ordinary characteristic $S(f) = b/f^2 + a/f^3$ and is nearly the same regardless of the observation node. Therefore, the analysis based on the variance of the common phase deviation is now applicable and provides the spectrum traced with solid line in Fig. 15, obtained for V_{GS} = -0.37 V. Saturation occurs at low frequency values, where it is not possible to carry out accurate measurements with

equipment available. In Fig. 16, the simulated and measured spectra can be compared with the ones obtained at V_{GS}=-0.8 V and with the distributed-line RTWO.

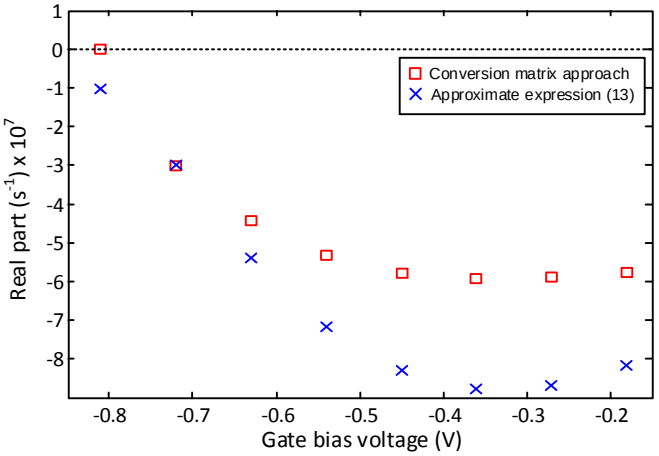

Figure 17. Differential-NLTL RTWO. Variation of the low magnitude negative real pole λ_2 versus the gate bias voltage.

VI. Conclusions

A new RTWO configuration based on the use of nonlinear transmission lines (NLTL) has been presented. The NLTL-based oscillator has been analyzed with harmonic balance, and its performance has been compared with that of a distributed-line RTWO. The NLTL-based RTWO provides quasi-square waveforms with a smaller number of gain stages. This is because the differential NLTL sharpens both the front and back portions of the waveform with the resulting reduction of rise and fall times. The coexistence of oscillation modes has been investigated with bifurcation-analysis techniques, obtaining, in the case of N = 2 gain stages, a coincident generation of the desired multiphase mode with an in-phase mode at the same Hopf bifurcation from dc regime. The phase-noise spectrum has been calculated numerically from the variance of the common phase deviation. The undesired effect of a real dominant pole has been investigated and mitigated with the aid of stability analysis tools.

Acknowledgment

The authors would like to thank to Dr. Sergio Sancho for his valuable help in the realization of this work and Spanish project TEC2011-29264-C03-01 for financial support.

References

[1] C. Cao and K. K. O, "Millimeter–wave voltage–controlled oscillator in 0.13–um CMOS technology," *IEEE J. Solid–State Circuits*, vol. 41, no.6, pp. 1297–1304, Jun., 2006.

[2] C.Y. Jeong and C. Yoo, "5–GHz low–phase CMOS quadrature VCO," *IEEE Microw. Wireless Compon. Lett.*, vol. 16, no. 11, pp. 609–611, Nov., 2006.

[3] A. Rofougaran, J. Rael, M. Rofougaran and A. Abidi, "A 900–MHz CMOS *LC*–oscillator with quadrature outputs," *IEEE Int. Solid–State Circuits Conf. Tech. Dig.*, CA, 1996, pp. 392–393.

[4] H. C. Choi, S. B. Shin and S. G. Lee, "A low–phase noise *LC*–QVCO in CMOS technology," *IEEE Microw. Wireless Compon. Lett.*, vol. 14, no. 11, pp. 540–542, Nov., 2004.

[5] S.C. Chan, P.J. Restle, K.L. Shepard, N.K. Jame and R.L Franch, "A 4.6 GHz resonant global clock distributed network," *IEEE Int. Solid–State Circuits Conf. Tech. Dig.*, 2004, vol. 1, pp.342–343.

[6] J. Kim and B. Kim, "A low phase–noise CMOS LC oscillator with a ring structure," *IEEE Int. Solid–State Circuits Conf. Dig. Tech.*, 2000, pp. 430–431.

[7] J. Savoj and B. Razavi, "A 10–Gb/s CMOS clock and data recovery circuit with frequency detection," *IEEE Int. Solid–State Circuits Conf. Dig. Tech.*, 2001, pp. 78–79.

[8] T.P. Liu, "A 6.5 GHz monolithic CMOS voltage–controlled oscillator," *IEEE Int. Solid–State Circuits Conf. Dig. Tech.*, 1999, pp. 404–405.

[9] J. Chien and L. Lu, "A 32–GHz rotary traveling–wave voltage controlled oscillator in 0.18–um CMOS," *IEEE Microw. Wireless Compon. Lett.*, vol.17, no.10, pp. 724–726. Oct., 2007.

[10] J. Wood, T. C. Edwards and S. Lipa, "Rotary traveling–wave oscillator arrays: A new clock technology," *IEEE J. Solid–State Circuits*, vol. 36, no. 11, pp. 1654–1665, Nov., 2001.

[11] G. Le Grand de Mercey, "A 18 GHz rotary traveling wave VCO in CMOS with I/Q outputs," *Proc. IEEE Eur. Solid–State Circuits Conf.*, 2003, pp. 489–492.

[12] J. Lee and B. Razavi, "A 40–Gb/s clock and data recovery circuits in 0.18– _m CMOS technology," *IEEE J. Solid–State Circuits*, vol. 38, no. 12, pp. 2181–2190, Dec., 2003.

[13] H. H. Hsieh, Y.C. Hsu and L. –H. Lu, "A 15/30–GHz dual–band multiphase voltage–controlled oscillator in 0.18–um CMOS," *IEEE Trans. Microw. Theory Tech.*, vol. 55, no. 3, pp. 474–483, Mar., 2007.

[14] N. Nouri and J. F. Buckwalter, "A 45–GHz rotary–wave voltage–controlled oscillator," *IEEE Trans. Microw. Theory Tech.*, vol.59, no.2. pp. 383–392, Feb., 2011.

[15] K. Takinami, R. Walsworth, S. Osman and S. Beccue, "Phase–noise analysis in rotary traveling–wave oscillators using simple physical model," *IEEE Trans. Microw. Theory Tech.*, vol.58, no.6, pp. 1465–1474, Jun., 2010.

[16] Y. Chen, "A low phase noise oscillator: rotary traveling wave oscillator," Ph.D., Dept. Elect. Eng., UC Santa Cruz, California, Dec., 2012.

[17] J. Guckenheimer and P. Holmes, *Nonlinear Oscillations, Dynamic Systems, and Bifurcations of Vector Fields*, Springer–Verlag, New York, 1983.

[18] J. Jugo, J. Portilla, A. Anakabe, A. Suárez and J.M. Collantes, "Closed–loop stability analysis of microwave amplifiers," *IEEE Electron. Lett.*, vol. 37, no. 4, pp. 226–228, 2001.

[19] J.M. Collantes, I. Lizarraga, A. Anakabe and J. Jugo. "Stability verification of microwave circuits through Floquet multiplier analysis," *Proc. IEEE Asia–Pacific Conf. Circuits Syst.*, Taiwan, 2004, pp. 997–100.

[20] V. Rizzoli, F. Mastri and D. Masotti, "General noise analysis of nonlinear microwave circuits by the piecewise harmonic–balance technique," *IEEE Trans. Microw. Theory Tech.*, vol. 42, no. 5, pp. 807–819, May 1994.

[21] M.G. Case and G. Raghavan, "Differential nonlinear tranmission line circuit," U.S. Patent 5789994 A, Aug., 4, 1998, [Online].

[22] M. J. W. Rodwell, S. T. Allen, R. Y. Yu, M. G. Case, B. Uddalak, R. Madhukar, E. Carman, M. Kamegawa, Y. Konishi, J. Pusl, and P. Rajasekhar, "Active and nonlinear wave propagation devices in ultrafast electronics and optoelectronics," *Proc. IEEE*, vol. 82, no. 7, pp. 1037–1056, Jul. 1994.

[23] E. Afshari and A. Hajimiri, "Nonlinear transmission lines for pulse shaping in silicon," *IEEE J. Solid–State Circuits*, vol. 40, no.3, pp. 744–752, Mar., 2005.

[24] B.Z. Essimbi and D. Jäger: "Generation of short electrical pulses and millimeter wave oscillations on a resonant tunnel diode nonlinear transmission line," *Current Applied Physics*, vol. 5, no. 6, pp. 567–571, Sep., 2005.

[25] J. M. Paillot, J. C. Nallatamby, M. Hessane, R. Quere, M. Prigent, and J. Rousset, "General program for steady state, stability, and FM noise analysis of microwave oscillators," *IEEE MTT–S Int. Microw. Symp. Dig.*, 1990, vol. 3, pp. 1287–1290.

[26] A. Demir. "Phase noise in oscillators: DAEs and colored noise sources," *IEEE/ACM Int. Conf. Comput. Aid. Des.*, pp. 170–177, 1998.

[27] A. Demir, A. Mehrotra, and J. Roychowdhury, "Phase noise in oscillators: a unifying theory and numerical methods for characterization," *IEEE Trans. Circuits Syst. I, Fundam. Theory Appl.*, vol. 47, May 2000.
[28] F. X. Kaertner, "Analysis of white and f −alpha noise in oscillators," *Int. J. Circuit Theory Appl.*, vol. 18, pp. 485–519, 1990.
[29] F. X. Kaertner, "Determination of the correlation spectrum of oscillators with low noise," *IEEE MTT–S Int. Microw. Symp. Dig.*, vol. 37, pp. 90–101, Jan 1989.
[30] A. Suárez, S. Sancho, S. Ver Hoeye and J. Portilla, "Analytical comparison between time– and frequency–domain techniques for phase–noise analysis," *IEEE Trans. Microw. Theory Tech.*, vol. 50, no.10, pp. 2353–2361, Oct., 2002.
[31] S. Sancho, F. Ramírez and A. Suárez, "Analysis and reduction of the oscillator phase noise from the variance of the phase deviations, determined with harmonic balance," *IEEE MTT–S Int. Microw. Symp. Dig.*, 2008, pp.1449–1452.
[32] S. Sancho, A. Suárez and F. Ramírez, "General phase–noise analysis from the variance of the phase deviation," *IEEE Trans. Microw. Theory Tech.*, vol.61, no.1, pp. 472–481, Jan., 2013.
[33] A. Suárez and R. Quéré, *Stability Analysis of Nonlinear Microwave Circuits*. Boston, MA: Artech House, 2003.
[34] A. Suárez, *Analysis and Design of Autonomous Microwave Circuits*. Hoboken, NJ: Wiley IEEE Pres, 2009.
[35] A. Suárez, J. Morales and R. Quéré, "Synchronization analysis of autonomous microwave circuits using new global–stability analysis tools," *IEEE Trans. Microw. Theory Tech.*, vol.46, no.5, pp.494–504, May, 1998.
[36] E. Palazuelos, A. Suárez, J. Portilla and F. J. Barahona, "Hysteresis prediction in autonomous microwave circuits using commercial software: application to a Ku–band MMIC VCO," *IEEE J. Solid–State Circuits*, vol.33, no.8, pp.1239–1243, Aug., 1998.
[37] T. S. Parker and L. O. Chua, *Practical Algorithms for Chaotic Systems*, Springer–Verlag, Berlin, 1989.
[38] F. Bonani and M. Gilli, "Analysis of stability and bifurcations of limit cycles in Chua's circuit through the harmonic–balance approach," *IEEE Trans. Circuits Syst. I*, vol.46, no. 8, pp. 881–890, 1999.
[39] N. V. Butenin, Y. I. Neimark, and N. A. Fufaev, *Introduction to the Theory of Non–Linear Oscillations* (in Spanish). Moscow, Russia: Mir, 1991.
[40] A. Demir, "Computing timing jitter from phase noise spectra for oscillators and phase–locked loops with white and 1/f noise," *IEEE Trans. Circuits Syst. I*, vol. 53, no. 9, pp. 1869–1884, Sep., 2006.
[41] C. Florian, P. A. Traverso, M. Feudale and F. Filicori, "A C–Band GaAs–pHEMT MMIC low phase noise VCO for space applications using a new cyclostationary nonlinear noise model," *IEEE MTT–S Int. Microw. Symp. Dig.*, Anaheim, 2010, pp. 284–287.
[42] A. Hajimiri and T.H. Lee, "A general theory of phase noise in electrical oscillators," *IEEE J. Solid–State Circuits*, vol.33, no.2, pp.179–194, Feb., 1998.
[43] M. Pontón, E. Fernández, A. Suárez and F. Ramírez, "Optimized design of pulsed waveform oscillators and frequency dividers," *IEEE Trans. Microw. Theory Tech.*, vol.59, no.12, pp.3428–3440, Dec., 2011.
[44] S. Sancho, A. Suárez, J. Domínguez and F. Ramírez, "Analysis of near–carrier phase–noise spectrum in free–running oscillators in the presence of white and colored noise sources," *IEEE Trans. Microw. Theory Tech.*, vol. 58, no.3, pp. 587–601, Mar., 2010.
[45] S. Sancho, A. Suárez and F. Ramírez, "Phase and amplitude noise analysis in microwave oscillators using nodal harmonic balance," *IEEE Trans. Microw. Theory Tech.*, vol. 55, pp. 1568–1583, 2007.
[46] F. Ramírez, M. Pontón, S. Sancho and A. Suárez, "Phase–noise analysis of injection–locked oscillators and analog frequency dividers," *IEEE Trans. Microw. Theory Tech.*, vol. 56, no.2, pp. 393–407, 2008.

Mabel Pontón (S'08–M'11) was born in Santander, Spain. She received the Telecommunication Engineering degree from the University of Cantabria, Spain in 2004, Masters in Information Technologies and Wireless Communications Systems and Ph.D. degree from the University of Cantabria, Santander, Spain, in 2008 and 2010, respectively. In 2006, she joined the Communications Engineering Department of University of Cantabria. Her research interests are focused on the nonlinear analysis and simulation of radiofrequency and microwave circuits, with emphasis on phase-noise, stability and bifurcation analysis of complex oscillator topologies.

Almudena Suárez (M'96–SM'01–F'12) was born in Santander, Spain. She received the Electronic Physics and Ph.D. degrees from the University of Cantabria, Santander, Spain, in 1987 and 1992, respectively, and the Ph.D. degree in electronics from the University of Limoges, Limoges, France, in 1993. She is currently a Full Professor with the Communications Engineering Department, University of Cantabria. She co-authored *Stability Analysis of Nonlinear Microwave Circuits* (Artech House, 2003) and authored *Analysis and Design of Autonomous Microwave Circuits* (IEEE-Wiley, 2009).
Prof. Suárez is a member of the Technical Committees of the IEEE Microwave Theory and Techniques Society (IEEE MTT-S) International Microwave Symposium (IMS) and the European Microwave Conference. She was an IEEE Distinguished Microwave Lecturer from 2006 to 2008. She is a member of the Board of Directors of the *European Microwave Association*. She is the Editor-in-Chief of the International Journal of Microwave and Wireless Technologies (Cambridge University Press). She was the co-chair of IEEE Topical Conference on RF Power Amplifiers (PAWR) in 2014.

J. Stevenson Kenney (S'84, M'85, SM'01, F'08) was born in St. Louis, MO, USA in 1962. He completed his B.S.E.E. (Hons.) in 1985 and M.S.E.E. in 1990, both from Georgia Institute of Technology. In 1994, he completed his Ph.D. in Electrical Engineering, also at Georgia Tech. In January 2000, Dr. Kenney joined the faculty at Georgia Institute of Technology, where he is currently a Professor in Electrical and Computer Engineering in the area of Electronics Design and Applications. He teaches and conducts research in the areas of power amplifier design and linearization, tunable RF materials and devices, and RFIC design. Dr. Kenney also has over 14 years of industrial experience in wireless communications. He has held engineering and management positions at Electromagnetic Sciences, Scientific Atlanta, and Pacific Monolithics, and Spectrian. Dr. Kenney has served as an expert witness on a number of patent litigations involving cellular telephone technology, and has testified four times at the U.S. International Trade Commission. He has been an active member of IEEE Microwave Theory and Techniques Society (MTT-S) for over 25 years. He served as an officer on the Santa Clara Valley chapter of MTT-S from 1996-2000. Dr. Kenney served three terms on the MTT-S AdCom. He served as Treasurer for 2001-2003, and was elected as MTT-S President in 2007. Dr. Kenney served on International Microwave Symposium (IMS) Steering Committees in Atlanta in 1993, San Francisco in 1996, Atlanta in 2008, and is currently General Co-Chair of IMS-2021, to be held in Atlanta. He has authored or co-authored more than 150 peer reviewed technical papers and conference papers in the areas of acoustics, analog/RF IC design, microwave system design, signal processing, and telecommunications. He has served on the Editorial Board for the *Transactions on Microwave Theory and Techniques* and the *Microwave and Wireless Components Letters* since 1997, and served on the IMS Technical Program Committee from 1997-2004, and 2010-present. Dr. Kenney received the 2005 IEEE MTT-S Application Award "for the development of power amplifier linearization techniques and insertion into cellular/wireless systems." In 2008, Dr. Kenney was elevated to IEEE Fellow "for contributions to microwave power amplifier design, characterization, and linearization."